•机械工程•

DOI:10.12454/j.jsuese.202400116

本刊网刊

柔性太阳翼毯面缝纫连接装配的拉伸性能研究

焦云雷[1],郭晨亮[1],冯世绪[1],吴跃民[2],左杨杰[3*]

(1.天津航天机电设备研究所,天津 300301;2.北京空间飞行器总体设计部,北京 100094;3.四川大学 空天科学与工程学院,四川 成都 610065)

摘　要:为了提高聚酰亚胺复合材料柔性薄膜连接性能,本文开展了柔性太阳翼毯面缝纫连接方法及拉伸性能试验研究,利用非接触应变测量技术(DIC)评估了连接拉伸失效特征,并探索了缝纫参数对连接性能的影响规律。结果表明:聚酰亚胺纤维织物复合材料板缝纫接头拉伸力和位移响应特征先呈现线性增长,随后达到失效强度,缝合孔周围应力集中明显,横向纤维束拉伸剥离,力随位移的增加波浪形下降且下降速率不断加剧;所有缝合接头失效模式相似,拉伸过程和最终失效后试件均发生严重褶皱,缝合区横向丝束间树脂强度较低导致大量丝束被拉伸剥离,但纤维丝束剥离仅发生在缝合区;4 mm缝合线迹对应的缝合接头最大拉伸载荷值均值最高,线迹长度越短,最大拉伸载荷值的均值趋向越大;50%位错较25%位错可以获得更大的最大拉伸载荷值均值;8 mm缝合线迹对应的试件除发生褶皱和横向纤维束剥离外,试件缝合区域两端均发生了缝线拉脱。所有缝合参数下试件拉伸滑移量均低于0.2 mm,随着拉伸次数增加滑移均值呈现出较弱的上涨趋势,缝合区表现出刚度退化的迹象;拉伸加载后,缝合区无论正面或背面均未发生胶层剥离、表面开裂、纤维剥离等现象,缝合连接方法表现出较高可靠性和刚度。

关键词:太阳翼;柔性薄膜;聚酰亚胺;复合材料;缝合连接;拉伸性能

中图分类号:V465　　**文献标志码:**A　　**文章编号:**2096-3246(2025)06-0344-08

轻质薄壁结构在航天领域被广泛应用[1–2],聚酰亚胺薄膜结构是轻质薄壁结构的典型代表,该结构优异的力学性能、绝佳的热稳定性和突出的耐化学性,使其成为太空探测器“防护服”的绝佳材料[3–5]。近年来,轻质薄壁结构被广泛应用于太空探测领域的研究[6],如柔性太阳能电池基板[7]、太阳帆[8]、太空望远镜[9–10]等。随着航天技术的飞速发展,对聚酰亚胺薄膜也提出了更高的要求,如轻量化、高比强度、可折叠等。其中,大体积航天器是未来航天技术发展的重要趋势之一[11–12],而为了满足制造、折叠等要求,其装配连接无法避免。然而,一方面,连接破坏了结构完整性,导致承载性能下降;另一方面,连接部位引入应力集中,极易导致结构局部损伤甚至灾难性破坏[13–15]。因此,发展航天聚酰亚胺薄膜材料先进装配连接技术对于保证中国大体积航天器研制具有非常重要的意义。

当前,装配连接方法有多种且各具优点:焊接气密性高[16–17],胶接轻量化水平好[18–19],螺接简单可靠[20–21],铆接低成本、高可靠[22–23]。此外,混合连接亦是提高连接性能的有效途径[24–25]。然而,航天聚酰亚胺薄膜材料结构属于典型的轻薄柔性材料[26],胶接成为其较合适的连接方法,而胶接热稳定差、工艺难控制、易老化[27],难以广泛、大量适用。尽管聚酰亚胺薄膜可以焊接[28],但聚酰亚胺薄膜通常以复合材料的形式出现[29–30],导致焊接难以适用。缝纫技术是连接薄壁材料的有效途径,但关于聚酰亚胺薄膜材料缝纫的研究报道十分稀少。

综上所述,本文开展了聚酰亚胺薄膜复合材料结构缝纫连接拉伸性能试验研究,揭示相关连接失效模式,评估不同连接参数对连接构件拉伸性能影响规律,为航天大型可展开结构研制提供装配连接技术参考。

收稿日期:2024 – 02 – 19　　**修回日期:**2024 – 09 – 13　　**网络出版日期:**2024 – 09 – 29

基金项目:天津市自然科学基金(22JCZDJC00940)

作者简介:焦云雷(1981—),男,研究员. 研究方向:航天器先进装配制造. E-mail:HT518JYL@163.com

* **通信作者:**左杨杰,副教授,E-mail:zuoyangjie@scu.edu.cn

1　试验准备

1.1　试件设计

为了实现轻量化、大面积，太阳翼聚酰亚胺薄膜复合材料结构厚度很小，常用的机械连接和焊接难以适用，同时，该类结构需在太空高低温、强辐射环境中服役，胶接亦不适用。

为此，本文开展薄膜缝纫连接方法研究，试件几何详细如图 1 所示。试件由聚酰亚胺薄膜纤维织物增强复合材料板制作而成，用两块复合板以单搭接方式拼接，缝合速度 6 针/s，针头采用 75 号针（参考标准 QB/T2255–96），针孔宽 0.32 mm，长 0.80 mm。缝线为高性能聚酰亚胺缝纫线，材料牌号为 ST–S30–200D×3，缝纫线直径 0.3～0.4 mm。缝线构型为 301 型线迹，线迹长度 L 是指两个相邻针眼之间的距离，一条线迹的针迹相对于另一条线迹的针迹具有一定的偏移量 a，定义双线位错为 $a/L\times100\%$。缝合完成后，缝合区域正面和背面均进行刷胶强化。

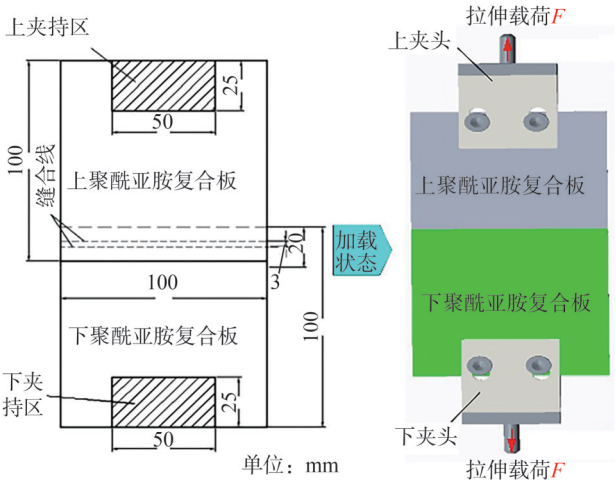

图 1　试件几何详细

Fig. 1　Geometrical details of the specimen

试件长度和宽度均为 100 mm，拉伸夹持区长为 50 mm、宽为 25 mm。试件材料为聚酰亚胺纤维织物增强复合材料，是将聚酰亚胺纤维通过机械编织工艺制成一定密度的聚酰亚胺纱织物与一定厚度的聚酰亚胺膜，并采用手工铺层，通过涂刷一定量室温硫化硅橡胶（RTV）胶粘接，在一定温度和压力条件下固化成型的复合材料。为了研究缝合参数对试件拉伸性能的影响，选择双线位错分别为 50% 和 25% 进行研究，同时线迹长度分别选择 4、6 和 8 mm。（针迹是缝针穿刺缝料时，在缝料上形成的针眼）。每个同条件试验重复 3 次，参数研究编号及参数大小如表 1 所示。

表 1　试件测试详细

Tab. 1　Details of specimens

编号	位错/%	线迹/mm	数量/件
4–50%	50	4	3
6–50%	50	6	3
8–50%	50	8	3
4–25%	25	4	3
6–25%	25	6	3
8–25%	25	8	3

1.2　试验过程

1.2.1　试验系统构成

为了评估构件缝合连接性能，分别开展拉伸性能测试试验和拉伸滑移测试试验。拉伸性能测试系统包括拉伸试验机、3 维非接触应变测量装置，目的在于测试构件连接力–位移相应特征和拉伸失效过程特征。拉伸滑移测试系统与拉伸测试系统相同，但加载方式采用多次重复加载，目的在于测试多次加载下连接接头滑移情况。

1.2.2　拉伸失效

拉伸失效试验现场如图 2 所示，采用型号为 AG–IC 的电子万能试验机进行拉伸试验，试验过程中所拍摄照片分别采用非接触应变测量技术（DIC）进行处理。拉伸速度为 1 mm/min，加载力范围为 1～1 000 N。试样夹持宽度限定为 50 mm。检查上下拉伸工装对正，调节上下端安装位置，保证固定后试件不受张力。将安装时要求用于固定的 4 个螺钉在加载力时按照顺序依次均匀小范围加载，保证被固定的试件正面无褶皱且除被加压应力外无其他应力，将拉力机拉力清零并移走压板。当试样沿针孔横向丝束剥离，出现明显滑移或拉脱时记录最大载荷值。

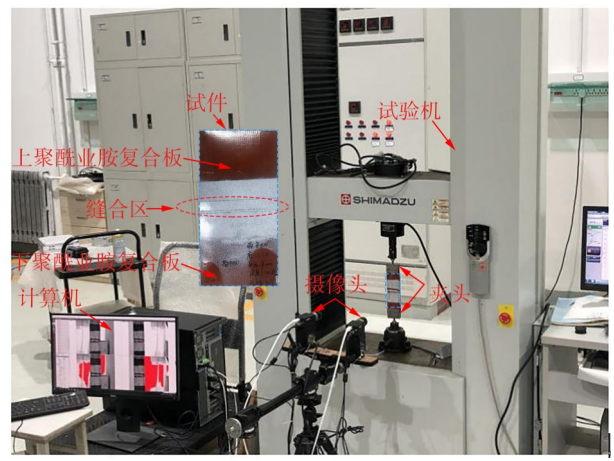

图 2　试件拉伸测试现场

Fig. 2　Tension test of the specimen

1.2.3　拉伸滑移

根据工程实践，在最大加载拉力为 5 N 下进行拉伸滑移测试。同样采用型号为 AG–IC 的电子万能试验机，试验过程摄照片采用 DIC 处理。每个试件加载

到 5 N 后就进行卸载，再重复加载和卸载 2 次，拉伸试验机从 0.5～5.0 N 依次加载力记录试样位移变化数据，记录最大位移值，要求 5 N 时最大位移值不大于 0.2 mm。拉伸滑移加载条件要求与拉伸试验相同，试件编号及参数如表 1 所示，相同参数（表 1）下重复测试 3 次。

2 试验结果分析

2.1 拉伸失效

2.1.1 力–位移响应

聚酰亚胺纤维织物复合材料板缝纫接头拉伸失效过程中力–位移响应曲线相似，典型的力–位移的响应曲线如图 3 所示。由图 3 可知，拉伸失效过程中，曲线呈现出明显的线性增长阶段和波浪形失效阶段：拉伸加载初期，力刚随位移线性增长，复合材料板和缝纫接头均处于弹性变形状态；随后，外载荷达到失效强度，此时缝合区域连接孔承受较大局部载荷，缝合孔垂直于拉伸方向的横向纤维束被拉伸剥离，力随着位移的增加呈现出波浪形下降；最后，缝合区破坏加剧，力随着位移增长而下降的趋势更加明显。

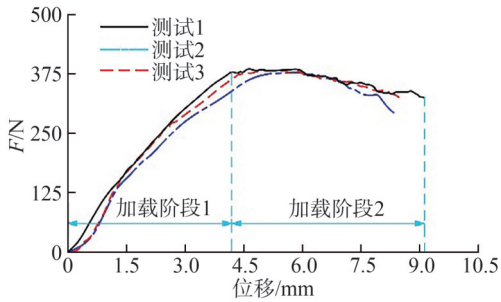

图 3 6–50% 试件力–位移响应曲线

Fig. 3 Load-displacement responses of 6–50% specimens

2.1.2 失效模式

接头典型失效模式如图 4 所示。由图 4 可知，拉伸加载后，由于缝线传载的应力集中，整体试件表面均发生了严重的褶皱。事实上，在拉伸失效发生前，试件表面因连接孔局部应力集中已经发生了褶皱。此外，缝合区由于横向丝束在拉伸方向上通过树脂传载，传载能力最弱，为此大量丝束被拉伸剥离，同时，缝合区表面涂胶层也发生破坏。值得注意的是，纤维丝束剥离仅发生在缝合区，缝合接头应力集中是主要原因，其他区域抗拉伸失效性能明显更好。

图 4 6–50% 试件失效模式

Fig. 4 Failure models of 6–50% specimens

2.1.3 失效过程

接头典型失效过程如图 5 所示。由图 5 可知：加载初期，缝口端部局部应变最大，很快就发生局部表面胶层破坏（图 5(b)）；随着外载增加，缝合线迹周围局部应

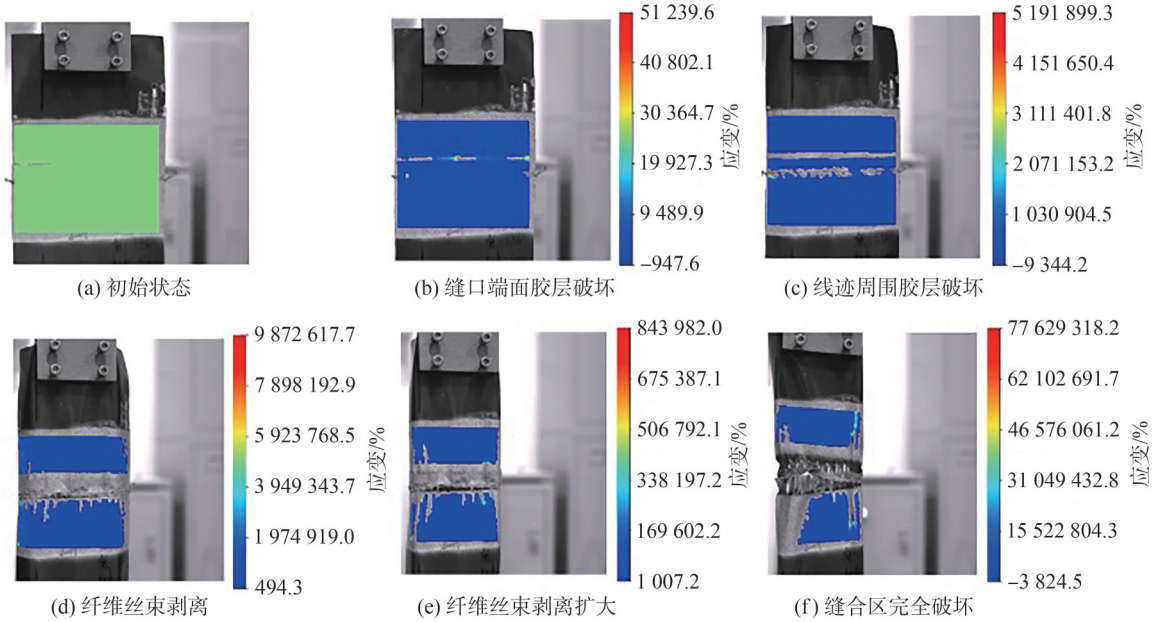

(a) 初始状态 (b) 缝口端面胶层破坏 (c) 线迹周围胶层破坏

(d) 纤维丝束剥离 (e) 纤维丝束剥离扩大 (f) 缝合区完全破坏

图 5 6–50% 试件失效过程模式

Fig. 5 Failure models of 6–50% specimens

变进一步增大，并伴随缝合区胶层破坏（图5(c)）；随后，缝合区纤维束发生剥离并进一步加剧（图5(e)）；最终，缝合区纤维束完全剥离，缝合接头完全分离失效（图5(f)）。

进一步分析试件垂直于表面方向的位移可知，加载过程中试件发生了明显的、变化的褶皱现象，如图6所示，其中，U_z是结构沿Z轴方向（垂直于拉伸方向）的位移大小。由图6可知：加载初期试件表面发生凸起，并未发生褶皱（图6(b)）；但当载荷进一步升高时，试件表层发生明显褶皱，且褶皱方向均往拍摄方向凸起（图6(c)）；随后，褶皱加剧，中间区域仍然向拍摄方向凸起，但边缘向后凹陷（图6(d)）；最后，褶皱程度达到最大值（图6(e)），并在随后的加载中因试件的破坏而进一步减小（图6(f)）。

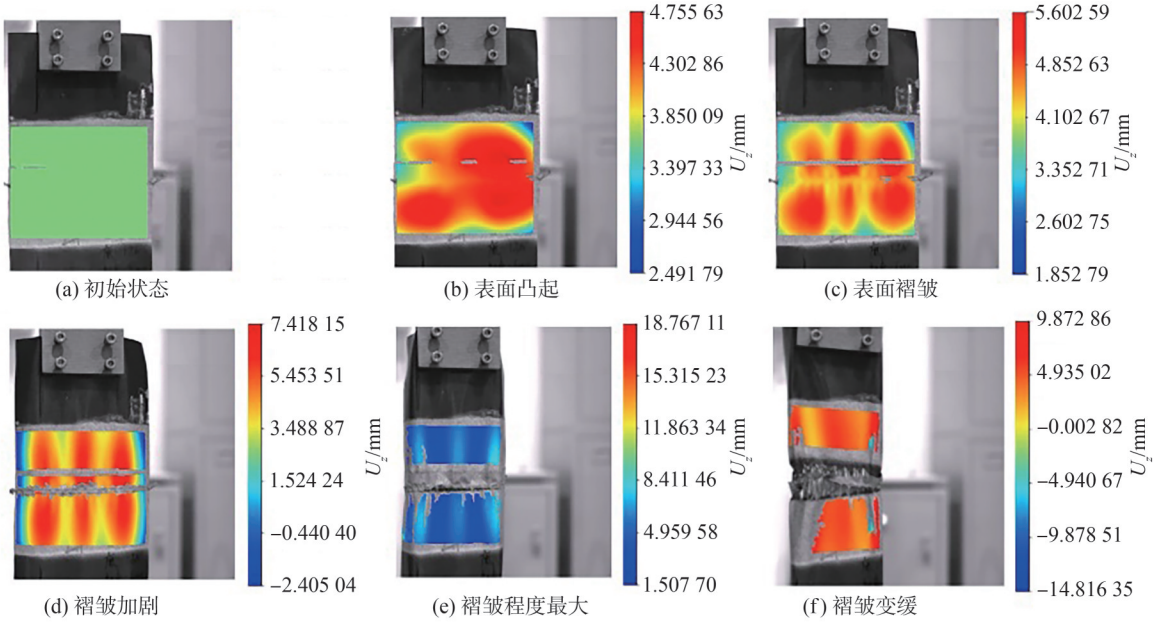

图6　6–50%试件拉伸过程中褶皱

Fig. 6　Folding progress of 6–50% specimens during tension loading

2.1.4　参数分析

为了优化缝合连接参数，对缝合线迹长度和双线位错进行分析。图7为不同位错、缝合线迹长度下最大载荷分布。由如图7可知：4 mm缝合线迹长度下缝合接头最大拉伸载荷值均值最高。且整体而言，线迹长度越短，最大拉伸载荷值的均值趋向越大。这很可能因为缝合线迹变短，相同缝纫长度下连接孔位增加，拉伸载荷下缝合区传载分散度更高、更均匀，连接孔局部最大应力水平下降，进而延缓了缝合区拉伸破坏。双线位错来看，50%位错较25%位错可以获得更大的最大拉伸载荷值均值，这很可能亦因为位错改变了缝合孔周围局部应力分布及孔周传载相互作用关系，更准确的原因和位错优化有待进一步借助有限元方法研究。

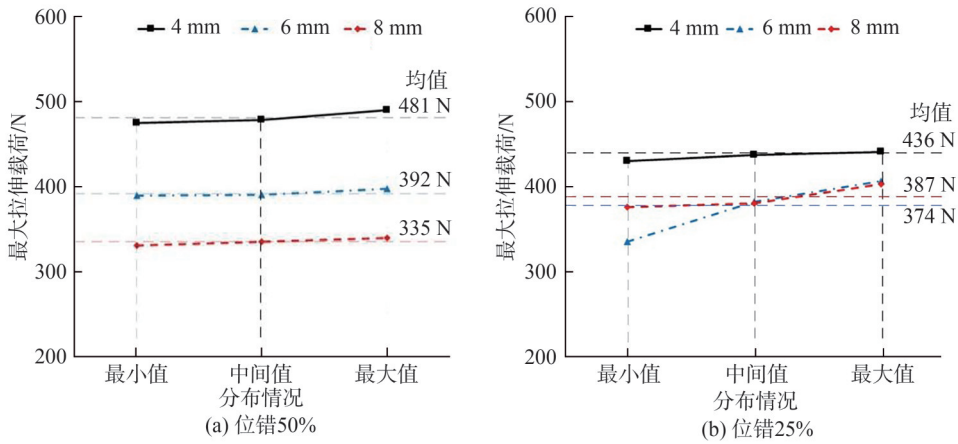

图7　不同参数下最大载荷分布

Fig. 7　Distributions of peak loads of specimens corresponding to different parameters

拉伸失效过程中，不同参数下的试件失效模式均相似。8 mm线迹下试件典型失效模式如图 8 所示。但值得注意的是，8 mm缝合线迹时所有试件除发生褶皱和横向纤维束剥离外，试件缝合区域两端均发生了缝线拉脱。其主要原因很可能是线迹太长，相同传载条件线缝合孔承受局部载荷更大，尤其是缝合区两端缝线相对约束力更小，最终发生了缝线拉脱。

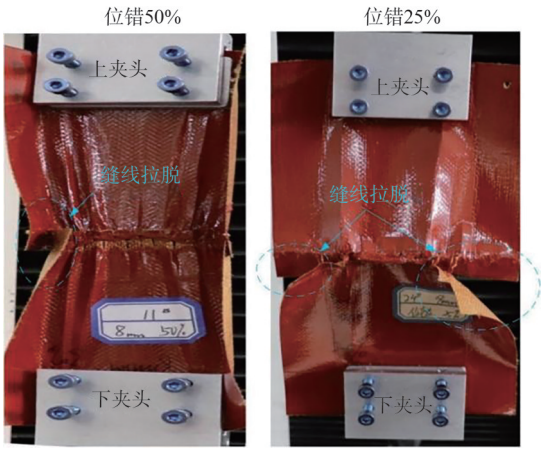

图 8　8 mm线迹下试件典型失效模式

Fig. 8　Typical failure models of 8 mm specimens

2.2　拉伸滑移

2.2.1　滑移分析

拉伸滑移试验过程中，所有缝合参数下的试件拉伸滑移量均低于 0.2 mm，满足工程中抗滑移要求。以 50% 位错下滑移量为例，随机选择同一材料板不同位置试件（试件 1、2、3），分析试件拉伸滑移量分布，结果如图 9 所示。图 9 中，均值为试件 1、2、3 的平均值。由图 9 可知，所有线迹长度下拉伸 3 次重复拉伸下滑移位移量均值均在 0.10～0.14 mm 范围内，表明缝合区域具有较好的刚度。与此同时，随着拉伸次数的增加，滑移均值呈现出较弱的上涨趋势，缝合区表现出刚度退化的迹象。

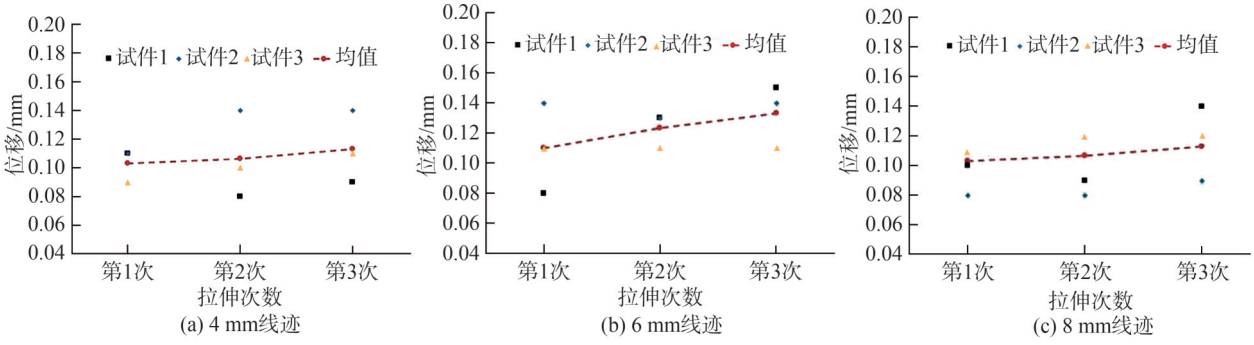

图 9　50% 位错下试件拉伸滑移量分布

Fig. 9　Tension displacement distributions of specimens corresponding to the dislocation level of 50%

2.2.2　接头表面

拉伸滑移测试后，观察缝合区胶层与基底材料及缝线粘接情况。典型的试件缝合区表面状态如图 10 所示，如 4 mm–50%–正面，表示缝合线迹长度为 4 mm、位错为 50% 的缝合区正面表面。由图 10 可知，拉伸加载后，缝合区无论正面或背面均未发生胶层剥离、表面开裂、纤维剥离等现象，表面缝线和涂胶状态完好，缝合连接状态未发生变化。可以看出，在要求的载荷水平下，缝合连接方法具有较好的可靠性和刚度。

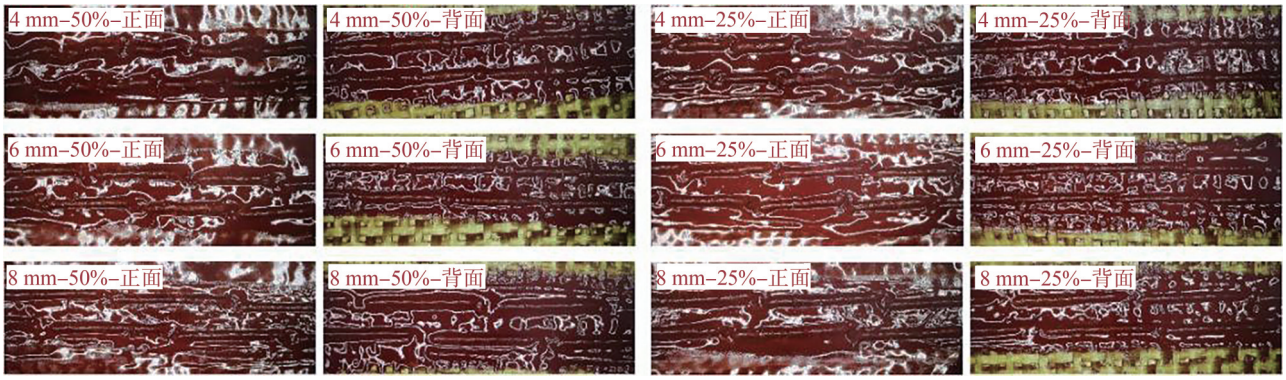

图 10　拉伸加载后缝合区表面状态

Fig. 10　Sewing area surfaces of specimens after tensile loading

3　结　论

1）聚酰亚胺纤维织物复合材料板缝纫接头拉伸失效过程，力–位移曲线先呈现出线性增长特征，复合材料板和缝纫接头均处于弹性变形状态，随后达到失效强度，缝合孔周围横向纤维束拉伸剥离，力随位移

的增加波浪形下降，并随位移的进一步增长下降趋势越来越明显。

2）所有缝合接头失效模式相似，拉伸过程和最终失效后试件均发生严重褶皱，缝合区由于横向丝束间树脂强度较低，大量丝束被拉伸剥离，但纤维丝束剥离仅发生在缝合区，其他区域抗拉伸失效性能明显更优。

3）4 mm缝合线迹长度下，缝合接头最大拉伸载荷值均值最高，且整体而言，线迹长度越短，最大拉伸载荷值的均值趋向越大；50% 位错较25% 位错可以获得更大的最大拉伸载荷值均值；8 mm缝合线迹对应的试件除发生褶皱和横向纤维束剥离外，试件缝合区域两端均发生了缝线拉脱。

4）所有缝合参数下，试件拉伸滑移量均低于0.2 mm，随着拉伸次数增加，滑移均值呈现出较弱的上涨趋势，缝合区表现出刚度退化的迹象；拉伸加载后，缝合区无论正面或背面均未发生胶层剥离、表面开裂、纤维剥离等现象，缝合连接方法表现出较高的可靠性和刚度。

参考文献：

[1] Wang Bo, Hao Peng,Tian Kuo, et al.Advances in lightweight design and experimental methods for aerospace structures[J].Journal of Astronautics,2023,44(4):596–606.[王博,郝鹏,田阔,等.航空航天结构轻量化设计与实验方法研究进展[J].宇航学报,2023,44(4):596–606.]

[2] Liu Hao, Liu Shanghe, Su Yintao, et al.Electrostatic discharge protection of spacecraft solar cell array based on meshed ITO film[J].Acta Aeronautica et Astronautica Sinica,2015,36(10):3494–3500.[刘浩,刘尚合,苏银涛,等.基于网格状ITO薄膜的航天器太阳电池阵静电放电防护[J].航空学报,2015,36(10):3494–3500.]

[3] Gao Hong,Wang Yongjian,Xing Yan,et al.The application and the development of high performance polyimide film in aerospace field[J].Spacecraft Environment Engineering,2014,31(3):248–253.[高鸿,王永建,邢焰,等.空间领域用高性能聚酰亚胺薄膜现状与发展[J].航天器环境工程,2014,31(3):248–253.]

[4] Wang Lei,Qing Fengling,Fan Hanlin.Properties of new polyimide film for spacecraft[J].Chinese Journal of Space Science,2012,32(6):869–873.[王磊,卿凤翎,范含林.航天器用新型聚酰亚胺薄膜性能研究[J].空间科学学报,2012,32(6):869–873.]

[5] Xu Zhen,Croft Z L,Guo Dong,et al.Recent development of polyimides:Synthesis,processing,and application in gas separation[J].Journal of Polymer Science,2021,59(11):943–962.

[6] Sezer Hicyilmaz A,Celik Bedeloglu A.Applications of polyimide coatings:A review[J].SN Applied Sciences,2021,3(3):363.

[7] Zhao Huiyang,Wang Hao,Zhao Liangliang,et al.Research process of flexible encapsulation materials and technology for space solar cells[J].Materials Reports,2022,36(22):23–33.[赵会阳,王豪,赵亮亮,等.空间太阳电池柔性封装材料与技术研究进展[J].材料导报,2022,36(22):23–33.]

[8] Liu Jikui, Zhang Kemo,Liu Qing, et al.Internal charging and discharging tests of large power transfer dielectric on spacecraft[J].High Voltage Engineering,2018,44(3):864–869.[刘继奎,张可墨,柳青,等.航天器大功率传输介质深层充放电试验研究[J].高电压技术,2018,44(3):864–869.]

[9] Zhang Peng,Jin Guang,Shi Guangfeng,et al.Current status and research development of space membrane reflectors[J].Chinese Journal of Optics and Applied Optics,2009,2(2):91–101.[张鹏,金光,石广丰,等.空间薄膜反射镜的研究发展现状[J].中国光学与应用光学,2009,2(2):91–101.]

[10] Wang Ruoqiu,Zhang Zhiyu,Xue Donglin,et al.Large-diameter high-efficiency diffractive Fresnel membrane elements for space telescope[J].Infrared and Laser Engineering,2017,46(9):0920001.[王若秋,张志宇,薛栋林,等.用于空间望远镜的大口径高衍射效率薄膜菲涅尔衍射元件[J].红外与激光工程,2017,46(9):0920001.]

[11] Wang Changguo,Wei Jianzheng,Liu Yuyan,et al.Some advances in technologies of aerospace flexible deployable structure and their applications[J].Journal of Astronautics,2020,41(6):761–769.[王长国,卫剑征,刘宇艳,等.航天柔性展开结构技术及其应用研究进展[J].宇航学报,2020,41(6):761–769.]

[12] Zhang Yuanxun, Xu Liping, Chen Guohui, et al. Analysis and application of folding and unfolding principle of spacecraft large-scale components[J].Chinese Space Science and Technology,2022,42(4):129–145.[张元勋,徐莉萍,陈国辉,等.航天器大尺度部件折叠展开原理分析及应用[J].中国空间科学技术,2022,42(4):129–145.]

[13] Wu Guoguang. Polyimide film and it's applications in aerospace[J].Information Recording Materials,2012,13(1):28–34.[吴国光.聚酰亚胺及其薄膜在航空航天中的应用[J].信息记录材料,2012,13(1):28–34.]

[14] Cui Junjia, Qi Lin, Jiang Hao, et al. Numerical and experimental investigations in electromagnetic riveting with different rivet dies[J].International Journal of Material Forming,2018,11(6):839–853.

[15] Repetto E A,Radovitzky R,Ortiz M,et al.A finite element study of electromagnetic riveting[J].Journal of Manufacturing Science and Engineering,1999,121(1):61–68.

[16] Zhang Qiliang,Cao Zengqiang,Qin Longgang,et al.Numerical simulation of electromagnetic riveting for titanium alloy[J].Rare Metal Materials and Engineering,2013,42(9):

1832–1837.[张岐良,曹增强,秦龙刚,等.钛合金电磁铆接数值模拟[J].稀有金属材料与工程,2013,42(9):1832–1837.]

[17] Li Keqin, Liu Zhihua, Zhou Liangang. Application status and development trend of Chinese aerospace welding technology[C]//International Forum on Aerospace Welding. Chinese Mechanical Engineering Society. Beijing: CMES, 2004: 68–74.[厉克勤,刘志华,周炼刚.中国航天焊接技术应用现状及发展趋势[C]//2004 航空航天焊接国际论坛论文集.北京:中国机械工程学会,2004:68–74.]

[18] Hachenberg D,Lavinge V,Mathe M.Crashworthiness of fuselage hydrid structure[C]//The 8th Triennial International Aircraft Fire and Cabin Safety Research Conference. Washington DC:FAA,2016:1–16.

[19] Shi Yalong,Wu Yaoyong,Wang Zhiyu,et al.Study on shear mechanical properties of steel-glass end-bonded joints[J]. Advanced Engineering Sciences, 2017(Supp2): 107 – 114.[史亚龙,吴耀勇,王志宇,等.钢–玻璃端面胶接接头剪切力学性能研究[J].工程科学与技术,2017(增刊2):107–114.]

[20] Kelly G.Load transfer in hybrid (bonded/bolted) composite single-lap joints[J].Composite Structures,2005,69(1):35–43.

[21] Xiong Feng,Wang Zhaoqiang,Ran Mingming,et al.Lateral stiffness of bolted prefabricated concrete wall[J]. Advanced Engineering Sciences,2022,54(3):98–108.[熊峰,王兆强,冉明明,等.螺栓连接装配式墙板抗侧刚度研究[J].工程科学与技术,2022,54(3):98–108.]

[22] Yang Zhou, Jiang Ruisong, Zuo Yangjie. Riveting damage behavior and mechanical performance assessments of CFRP/CFRP single-lap gasket-riveted joints[J]. Engineering Failure Analysis,2023,149:107253.

[23] Zhang Liufeng, Liang Ying, Wang Yewei, et al. Research and application of rain proof sealing technology for riveted cabin of launch vehicle[J]. Aerospace Manufacturing Technology,2020(3):50–52.[张柳锋,梁莹,王业伟,等.运载火箭铆接舱体防雨密封技术研究及应用[J].航天制造技术,2020(3):50–52.]

[24] Ma Su, Zhao Qilin. Analysis of the bonded-bolted hybrid composite joints' carrying capacity[J].Acta Materiae Compositae Sinica,2011,28(4):225–230.[马毓,赵启林.复合材料胶–螺混合连接接头承载力分析[J].复合材料学报,2011,28(4):225–230.]

[25] Liu Lulu,Wang Xin,Wu Zhishen,et al.Resistance and ductility of FRP composite hybrid joints[J].Composite Structures,2021,255:113001.

[26] Liu Jingang, Ni Hongjiang, Gao Hong, et al. Research and application of ultrathin polyimide films[J]. Spacecraft Environment Engineering,2014,31(5):470–475.[刘金刚,倪洪江,高鸿,等.超薄聚酰亚胺薄膜研究与应用进展[J].航天器环境工程,2014,31(5):470–475.]

[27] Li Yingdong,Zhao Pizhi,Feng Yingjuan,et al.Influence of anodic oxide film structure on adhesive bonding performance of 5754 aluminum alloy[J].Transactions of Nonferrous Metals Society of China,2019,29(9):1836–1841.

[28] Yin Weida, Qin Mengmeng, Yu Huitao, et al. Hyperelastic graphene aerogels reinforced by in-suit welding polyimide nano fiber with leaf skeleton structure and adjustable thermal conductivity for morphology and temperature sensing [J].Advanced Fiber Materials,2023,5(3):1037–1049.

[29] Chen Beibei,Yang Bi,Tong Yang,et al.Enhanced tribological properties of polyimide composite with carbon fiber/graphitic-carbon nitride nanosheets[J]. Journal of Applied Polymer Science,2023,140(35):e54360.

[30] Yu Dingyi, Xue Tiantian, Ma Zhuocheng, et al. 3D printed polyimide/silica composite aerogels for customizable thermal insulation from −50 ℃ to 1300 ℃[J].Chinese Journal of Polymer Science,2024,42(7):936–945.

Study on Suture Tensile Properties of Polyimide Composites for Flexible Solar Wings

JIAO Yunlei[1], *GUO Chenliang*[1], *FENG Shixu*[1], *WU Yuemin*[2], *ZUO Yangjie*[3*]

(1.Tianjin Institute of Aerospace Mechanical and Electrical Equipment, Tianjin 300301, China;
2.Beijing Space Vehicle Overall Design Department, Beijing 100094, China;
3.School of Aeronautics and Astronautics, Sichuan University, Chengdu 610065, China)

Abstract:

Objective Polyimide fiber fabric composite laminate is a typical aerospace flexible film material. Achieving high-quality joining of these film composites remains challenging, and the joining quality has a significant influence on the service performance of spacecraft. This study investigates the sewing connection method of polyimide fiber fabric composite laminate used in the flexible solar wing blanket surface of spacecraft to improve the joining performance of these film composites.

Methods The sewing test of polyimide fiber fabric composite laminate is designed to evaluate the sewing quality of the joint. Both the tensile failure progression and final failure modes are characterized through quasi-static tensile tests. The surface tensile deformation of the specimen is evaluated using digital image correlation (DIC) measurement technology. In addition, parameter tests of film sewing joints are conducted to examine the influence of sewing parameters on the connection performance, including sewing dislocation and sewing stitches. Finally, the tensile slip

performance of the specimen is assessed through tensile slip tests, in which different sewing parameters are also considered.

Results and Discussions During the tests, adhesive layer peeling, surface cracking, and fiber peeling in the sewing area are examined. The tensile load-displacement results show that the tensile failure process of the sewing joint of polyimide fiber fabric composite laminate exhibits a linear growth characteristic in the force–displacement curve. Both the composite material laminate and the sewing joint remain in an elastic deformation state until the failure strength is reached, leading to multiple failure modes in the joint. The parameter study indicates that the highest average maximum tensile load of the specimen corresponds to a suture stitch length of 4 mm. In addition, the shorter the suture stitch length, the higher the average maximum tensile load value. This behavior likely results from the shorter suture stitches increasing the number of joining holes when the sewing length remains the same. When the specimen is loaded, the load distribution in the suture zone becomes more uniform, and the local maximum stress level at the joining hole decreases, which in turn delays tensile failure in the suture area. From the perspective of two-line dislocation specimens, 50% dislocation yields a larger average maximum tensile load value than 25% dislocation. This is likely because the dislocation alters the local stress distribution around the suture hole and improves the joining interaction of the specimen, leading to changes in the load transfer condition. The tensile loading progression of the specimen shows that, due to the stress concentration carried by the sutures, the specimen surface becomes severely wrinkled. Before tensile failure occurs, the surface of the specimen becomes wrinkled due to local stress concentration at the connecting hole. In addition, the suture zone demonstrates the weakest load-bearing capacity because the transverse tow is carried through the resin in the tensile direction. Therefore, a large number of tows are stretched and peeled off, and the adhesive layer on the surface of the suture area is destroyed. Fiber tow peeling occurs only in the suture area, where stress concentration in the suture joint is the main cause. The tensile failure resistance in other areas remains significantly higher. At the initial loading stage, the local strain at the end of the seam is the largest, and the local surface adhesive layer is destroyed early. As the external load increases, the local strain around the suture stitch further increases, and the glue layer in the suture zone becomes damaged. Then, fiber bundles in the suture zone peel and progressively deteriorate. Eventually, the fiber bundles in the suture area completely peel off, leading to total separation and failure of the suture joint. During the tensile failure process, the failure modes of the specimens under different parameters are similar. However, when the stitches are sutured at 8 mm, all specimens are pulled off at both ends of the suture area, in addition to wrinkles and transverse fiber bundle peeling. The main reason is likely that the stitches are too long, causing the suture holes under the same load conditions to experience greater local loads. In particular, the sutures at both ends of the suture-bearing area are relatively less constrained, resulting in suture pull-off. Further analysis of the displacement of the specimen perpendicular to the surface shows that the specimen exhibits obvious and varying wrinkles during the loading process. At the beginning of loading, no wrinkles appear on the specimen surface. However, as the load increases, distinct wrinkles form, protruding in the shooting direction. Then, the folds intensify, the middle area remains convex in the shooting direction, and the edges become concave backward. Finally, the degree of wrinkling reaches a maximum and is later reduced due to specimen destruction during further loading. The tensile slip test shows that the tensile slip of the specimen under all suture parameters remains less than 0.2 mm, indicating that the suture area exhibits good stiffness. As the number of stretches increases, the mean slip value shows a weak upward trend, and the suture zone demonstrates slight stiffness degradation. After tensile loading, no adhesive layer peeling, surface cracking, or fiber peeling occurs in the sewing area on either side of the specimens.

Conclusions These results indicate that the sewing connection method demonstrates high reliability and stiffness in joining polyimide fiber fabric composite structures. This study provides valuable insights for the design of aircraft thin-wall composite structure joints.

Key words: solar wing; flexible film; polyimide; composites; stitched connections; tensile properties

（编辑　吴芝明）

引用格式：Jiao Yunlei, Guo Chenliang, Feng Shixu, et al. Study on suture tensile properties of polyimide composites for flexible solar wings[J]. Advanced Engineering Sciences, 2025, 57(6): 344–351. [焦云雷，郭晨亮，冯世绪，等. 柔性太阳翼毯面缝纫连接装配的拉伸性能研究[J]. 工程科学与技术，2025，57(6)：344–351.]